

Impact of phosphate adsorption on the mobility of PANI-supported nano zero-valent iron

Dantong Lin¹ | Scott Bradford² | Liming Hu¹  | Irene M. C. Lo³

¹ State Key Lab. of Hydro-Science and Engineering, Dep. of Hydraulic Engineering, Tsinghua Univ., Beijing 100084, China

² U.S. Salinity Lab., USDA-ARS, Riverside, CA 92507, USA

³ Dep. of Civil and Environmental Engineering, The Hong Kong Univ. of Science and Technology, Clear Water Bay, Sai Kung, Hong Kong, China

Correspondence

Liming Hu, State Key Lab. of Hydro-Science and Engineering, Dep. of Hydraulic Engineering, Tsinghua Univ., Beijing 100084, China.

Email: gehu@tsinghua.edu.cn

Assigned to Associate Editor Thomas Harter.

Funding information

National Natural Science Foundation of China, Grant/Award Numbers: Project No. 51661165015, 51979144; Open Research Fund Program of State key Laboratory of Hydrosience and Engineering, Grant/Award Number: Project No. SKLHSE-2019-D-03; Research Grants Council of Hong Kong Joint Research Scheme, Grant/Award Number: Project No. N_HKUST603/16

Abstract

Nano zero-valent iron (nZVI) has been used for in situ groundwater remediation due to its strong adsorption and reaction characteristics. However, oxyanion contaminants in groundwater can readily adsorb onto the surface of nZVI. This can potentially alter the mobility of nZVI and create a secondary pollution source, but these issues have not yet been systematically investigated. In this study, polyaniline-supported nZVI (PnZVI) and phosphate-sorbed PnZVI (PS-PnZVI) were synthesized in the laboratory. The sedimentation and transport behavior of these two nZVI particles were investigated, compared, and mathematically modeled to better understand the impact of phosphate adsorption on these processes. Results showed that phosphate adsorption can enhance the stability and mobility of PnZVI. Interaction energy calculations that considered van der Waals and magnetic attraction, electrostatic double layer and Born repulsion, and the influence of nanoscale roughness and binary charge heterogeneity were conducted to better infer mechanisms causing nZVI particle sedimentation and retention. Nanoscale roughness and binary charge heterogeneity were found to significantly decrease the energy barrier, but not to low enough levels to explain the observed behavior. The rapid settling of PnZVI was attributed to strong magnetic attraction between particles, which produced rapid aggregation and retention due to straining and/or hydrodynamic bridging. Phosphate adsorption enhanced the mobility of PS-PnZVI in comparison with PnZVI due to a decrease in particle size and aggregation, and an increase in the energy barrier with the porous media. A potential risk of nZVI particles to facilitate oxyanion contaminant transport was demonstrated for phosphate.

Abbreviations: ADE, advection–dispersion equation; BTC, breakthrough curve; CH, charge heterogeneity; DI, deionized; DLVO, Derjaguin–Landau–Verwey–Overbeek; EDS, energy dispersive spectrometer; ICP–OES, inductively coupled plasma optical emission spectroscopy; NR, nanoscale roughness; nZVI, nano zero-valent iron; PANI, polyaniline; PnZVI, polyaniline-supported nano zero-valent iron; PS-PnZVI, phosphate-sorbed nano zero-valent iron; PV, pore volume; RP, retention profile; SEM, scanning electron microscope; TEM, transmission electron microscope.

This is an open access article under the terms of the [Creative Commons Attribution](https://creativecommons.org/licenses/by/4.0/) License, which permits use, distribution and reproduction in any medium, provided the original work is properly cited.

© 2021 The Authors. *Vadose Zone Journal* published by Wiley Periodicals LLC on behalf of Soil Science Society of America

1 | INTRODUCTION

Groundwater contamination is one of the most severe environmental problems today and poses a threat to public health around the world (Khan, Husain, & Hejazi, 2004). Because of the huge amount of contaminated groundwater, in situ remediation is an economical way to solve this problem (Karn, Kuiken, & Otto, 2009). Over the last few decades,

nanomaterials have become an important aspect of in situ technologies for groundwater remediation due to their large specific area and strong adsorption capacity (Karn et al., 2009; Macé et al., 2006). Nano zero-valent iron (nZVI) is one of the most popular nanomaterials because of its low cost and toxicity (Chekli et al., 2016; Zhang, 2003), and high potential to remediate a wide range of aqueous contaminants, including different types of heavy metals and organics (Crane & Scott, 2012; Tosco, Petrangeli Papini, Cruz Viggi, & Sethi, 2014; Wang & Zhang, 1997).

One of the advantages of nZVI as an in situ remediation material is that it can be injected into groundwater, forming an effective reaction zone by moving with groundwater (Ling & Zhang, 2017). Previous studies suggested that the widespread application of nZVI was restricted because of its limited mobility. Several methods have therefore been developed to enhance the mobility of nZVI, such as the use of supporting polymers (Elliott & Zhang, 2003; Kanel, Goswami, Clement, Barnett, & Zhao, 2008; Kocur et al., 2014) or emulsifier (Su et al., 2013; Zhang, Dong, Gao, Cai, & Dong, 2019). Furthermore, researchers have investigated the influence of physical factors of the aquifer (such as soil grain size, groundwater velocity, and injection model) and geochemical conditions (such as solute concentration and humic acid) of groundwater to optimize the mobility of nZVI (Dong & Lo, 2014; Jiemvarangkul, Zhang, & Lien, 2011; Li, Zhao, Han, & Hong, 2015; Saberinasr, Rezaei, Nakhaei, & Hosseini, 2016; Saleh et al., 2008).

Organic contaminants can be degraded by nZVI through a reductive chemical reaction (Kaifas et al., 2014; Raychoudhury & Scheytt, 2013; Su et al., 2013). For example, Su et al. (2012) reported that emulsified zero-valent iron produces an 85% mass reduction of tetrachloroethene (PCE) in the field after 2.5 yr. Published results show that polymers can enhance the stability and mobility of nZVI (Cirtiu, Raychoudhury, Ghoshal, & Moores, 2011; Raychoudhury, Naja, & Ghoshal, 2010). Consequently, nZVI that has been stabilized by polymers can potentially remediate organic contaminants spread over a larger area. However, nZVI also has been used to remediate inorganic contaminants like arsenic and phosphate by adsorption (Almeelbi & Bezbaruah, 2012; Lin, Hu, Lo, & Yu, 2020; Lin, Zhang, & Hu, 2019). In this way, nZVI and sorbed contaminants on its surface can coexist in the subsurface system for a long time (Almeelbi & Bezbaruah, 2014). Adsorbed oxyanion contaminants on the surface of nZVI will continue to exist in the subsurface and may potentially change the mobility of nZVI. This study aimed to illustrate how the mobility of modified nZVI changes after the adsorption of phosphate.

The interaction energy between a particle and the solid-water interface is usually used to evaluate the mobility of colloids in porous media (Sasidharan, Torkzaban, Bradford, Cook, & Gupta, 2017; Tian, Gao, Silvera-Batista,

Core Ideas

- Enhanced negative zeta potential due to phosphate adsorption impedes aggregation.
- Phosphate adsorption on nZVI enhances its stability and mobility.
- Nanoscale roughness and chemical heterogeneity decrease the energy barrier due to DLVO theory.
- Potential risk of nZVI to facilitate contaminant transport should be of concern.

& Ziegler, 2010). Researchers have used the Derjaguin-Landau-Verwey-Overbeek (DLVO) theory to determine the interaction energy of nZVI (Phenrat et al., 2008). However, in previous work, both the surface of nZVI and solid-water interface were considered as smooth and chemical homogeneous. In recent years, the influence of nanoscale roughness and chemical heterogeneity on the interaction energy has been stressed by many researchers (Bendersky & Davis, 2011; Hoek, Bhattacharjee, & Elimelech, 2003). Nano zero-valent iron usually exists in water in the form of aggregates, which can have a rough surface. Besides, the uneven distribution of adsorbed ions on the nZVI surface can cause surface charge heterogeneity, especially for polymer-supported nZVI, because the ions are mainly sorbed by iron particles distributed on the polymer surface. Therefore, it is necessary to study the influence of nanoscale roughness and charge heterogeneity on the interaction energy of nZVI before and after the adsorption of contaminants.

Phosphorous is one of the primary nutrients for living species. However, excess phosphorus in water can cause eutrophication, which is one of the main water problems nowadays (Nagoya, Nakamichi, & Kawase, 2019). Nano zero-valent iron has been proved to have a high removal capacity for phosphate (Wen, Zhang, & Dai, 2014); therefore, the mobility of nZVI is expected to be influenced by phosphate sorption into groundwater. Furthermore, previous studies have shown that phosphate has similar geochemical behavior to arsenate (Antelo, Avena, Fiol, López, & Arce, 2005), which is one of the most toxic contaminants in groundwater. Phosphate and arsenate have similar structures, since phosphorus and arsenic are in the same element group, and they both have a relatively strong affinity for mineral surfaces like goethite (Antelo et al., 2005). The main mechanism of phosphate and arsenate removal by nZVI both include adsorption and coprecipitation (Sushil Raj, Jean-Mark, & Heechul, 2006; Zhang et al., 2017), and these two oxyanions are considered to compete for adsorption sites on nZVI surfaces (Dong, Guan, & Lo, 2012; Zhang et al., 2018). In view of the similarity of phosphate and arsenate, a study investigating the impact of phosphate

on nZVI mobility has important implications for arsenate-contaminated groundwater remediation.

In this study, polyaniline-supported nZVI (PnZVI) and phosphate-sorbed PnZVI (PS-PnZVI) were synthesized in the laboratory. The stability and the mobility of PnZVI and PS-PnZVI were compared in deionized (DI) water and saturated glass beads. Batch tests were carried out to demonstrate the adsorption capability of PnZVI for phosphate. Sedimentation tests were conducted to study the stability of the PnZVI and PS-PnZVI particles in water. Column tests were conducted to quantify the transport and retention process for PnZVI and PS-PnZVI particles. Interaction energy calculations that considered the influence of nanoscale roughness and charge heterogeneity were conducted to better understand mechanisms controlling particle retention and aggregation.

2 | MATERIALS AND METHODS

2.1 | PnZVI and PS-PnZVI

Nano zero-valent iron was synthesized in the laboratory before (denoted as PnZVI) and after (denoted as PS-PnZVI) phosphate adsorption. The PnZVI was synthesized using a liquid-phase reduction method (Bhaumik, Noubactep, Gupta, McCrindle, & Maity, 2015). In brief, 6 g of iron(III) chloride was dissolved in 80 ml DI water (produced by Milli-Q, Merck), contained in a 250-ml three-neck flask. Next, 0.8 ml aniline was added into the iron(III) chloride solution with magnetic stirring (600 rpm) for 5 min. After reaction for 2 d, 100 ml of 1 M sodium borohydride solution was added dropwise into the container with nitrogen protection. After reaction for 1 h, a black PnZVI powder was obtained by centrifugation and freeze drying. The PnZVI powder was dissolved in DI water and ultrasonicated for 2 h to form a well-dispersed suspension that was used in experiments described below.

The PS-PnZVI was prepared using an adsorption method (Yu, Hu, & Lo, 2019). First, 1 ml of monopotassium phosphate solution with a concentration of 2,000 mg L⁻¹ was added into 100 ml of 150-mg L⁻¹ PnZVI suspensions, then the mixed suspension was shaken for 1 h to reach equilibrium. The prepared PS-PnZVI was extracted using 0.45- μ m filter paper to minimize any excess phosphate in the suspension. A new suspension for transport studies was prepared by immediately transferring the filter paper with the PS-PnZVI into a new bottle of 100 ml DI water. The bottle was capped and hand shaken to separate the PS-PnZVI from the filter paper.

The morphology of PnZVI was examined with a scanning electron microscope (SEM, Merlin, Zeiss) and a transmission electron microscope (TEM, JEM-2010F, Japan Electron Optics Laboratory). An energy dispersive spectrometer (EDS) was used to analyze the element distribution of PnZVI and to confirm the adsorption of phosphate on PS-PnZVI.

All the reagents used in this study (iron(III) chloride, sodium borohydride, monopotassium phosphate, aniline, and nitric acid) were analytic grade obtained from Aldrich Chemical.

2.2 | Batch tests

Batch tests were conducted to investigate the adsorption capacity of phosphate on PnZVI in DI water. Dynamic batch experiments were carried out to study the kinetics of the phosphate adsorption process. In this case, the concentration of PnZVI suspension was 150 mg L⁻¹ and the initial concentration of phosphorus was 10 mg L⁻¹ (in the form of monopotassium phosphate solution). The concentration of phosphorous was measured at 5, 10, 20, and 30 min. Equilibrium batch adsorption tests were conducted to determine the maximum adsorption capacity of phosphate on PnZVI in DI water. The concentration of PnZVI suspension was 150 mg L⁻¹ in these experiments, and the initial concentration of phosphorus was 5, 10, 20, 30 and 50 mg L⁻¹ (in the form of monopotassium phosphate solution). The concentration of the phosphorus was measured using inductively coupled plasma optical emission spectroscopy (ICP-OES, Prodigy7, Teledyne Leeman Labs). Each batch test was repeated three times to get the mean value and standard deviation of the results.

2.3 | Particle size and zeta potential analyses

The initial particle size distribution of PnZVI and PS-PnZVI suspensions was measured by the wet laser diffraction particle characterization method with a Laser Particle Analyzer (Mastersizer 2000, Malvern Instruments) (Stutter & Richards, 2012). The particle size measurement was conducted within 10 min with mechanical stirring to avoid aggregation. The zeta potential of these suspensions was measured using the electrophoretic light scattering method (ELS) with a zeta potential analyzer (NanoBrook 90Plus Zeta, Brookhaven Instruments; Feng et al., 2015).

2.4 | Sedimentation tests

Sedimentation experiments were conducted to study the stability of PnZVI and PS-PnZVI suspensions in DI water. Experiments were conducted using an initial suspension concentration of 150 mg L⁻¹ and then measuring the optical absorbance every 5 min for 8 h. The optical density of suspensions was determined using ultraviolet spectrophotometry (DR5000, Hach) at a wavelength of 508 nm (Yin, Lo, Dong, Rao, & Mak, 2012). The concentration of suspended particles showed a linear relationship with the optical density; therefore, the change of optical density of a colloidal suspension

with time was used to describe the aggregation and sedimentation process (Phenrat, Saleh, Sirk, Tilton, & Lowry, 2007).

2.5 | Column tests

Column tests were conducted to examine the transport and retention behavior of PnZVI and PS-PnZVI. The test setup for the column experiments is shown in Supplemental Figure S1. The column with a length of 14 cm and an i.d. of 3 cm was filled with glass beads with a mean diameter of 613 μm . The pore volume (PV) of the glass bead-filled column was 35.25 ml. The top of the column was connected to a peristaltic pump (BT-100SD, Shanghai Huxi Analysis Instrument Factory). The flow rate of the injection is 5 ml min^{-1} and the approach velocity is 0.707 cm min^{-1} (10.2 m d^{-1}), which falls within the normal range used in column studies (Chrysikopoulos & Syngouna, 2014; Crampon et al., 2018). The bottom of the column was connected to an autosampler (BZS-100, Shanghai Huxi Analysis Instrument Factory), which collected the effluent in a small glass tube every 1 min to get the breakthrough curves (BTCs).

For each type of nZVI particle and a conservative tracer (potassium bromide solution), one PV of the suspension was injected from the top of the column, followed by five PVs of DI water. The effluent collected in the glass tubes was acidified and the concentration of potassium, iron, and phosphorus was measured by ICP (Prodigy7, Teledyne Leeman Labs). After the injection of nZVI and DI water, the liquid in the column was discharged and the solid in the column was excavated in 2-cm increments (2 cm \times 7 layers) and acidized to measure the retention profiles (RPs) of the nZVI in the column using the ICP. Each column test was repeated three times. The mean value and the standard deviation of the results are shown in the figures.

2.6 | Numerical model

The transport of nZVI particles in the porous medium was described using the advection–dispersion equation (ADE) with kinetic terms for retention and release of particles (Bradford, Šimůnek, Bettahar, van Genuchten, & Yates, 2003) as

$$\frac{\partial C}{\partial t} + \frac{\rho_b}{n} \left(\frac{\partial S}{\partial t} \right) = D \frac{\partial^2 C}{\partial x^2} - v \frac{\partial C}{\partial x} \quad (1)$$

$$\frac{\partial S}{\partial t} = \frac{n}{\rho_b} \psi k_{\text{att}} C - k_{\text{det}} S \quad (2)$$

where C (mg L^{-1}) is the liquid-phase concentration of nZVI, S (mg g^{-1}) is the solid phase concentration of nZVI, ρ_b (kg m^{-3}) is the bulk density of the porous medium, D ($\text{m}^2 \text{s}^{-1}$) is the dispersion coefficient, x (cm) is the space coordinate, t (min)

is the time, n (–) is the porosity of the glass bead, v (m s^{-1}) is the pore water velocity, k_{att} (s^{-1}) and k_{det} (s^{-1}) are the first-order retention and release coefficients, respectively, and ψ is a dimensionless function that accounts for nonexponential retention processes. The value of ψ is given as

$$\psi = \left(\frac{d_c + x}{d_c} \right)^{-\beta} \quad (3)$$

where d_c (μm) is the median size of the glass beads, and β is a constant which governs the hyper-exponential shape of the RPs that was taken as 0.432 (Liang, Bradford, Šimůnek, Vereecken, & Klumpp, 2013). The parameter ψ portrays space-dependent retention behavior such as hydrodynamic bridging or straining (Bradford et al., 2003).

HYDRUS-1D software was used to numerically solve Equations 1–3 in this study (Bradford et al., 2003). A piecewise-constant concentration boundary was used as the upper boundary condition, which can be written as

$$\begin{aligned} C(0, t) &= C_0, 0 < t < t_0 \\ C(0, t) &= 0, t_0 < t < t_{\text{end}} \end{aligned} \quad (4)$$

where C_0 is the initial concentration equal to 150 mg L^{-1} , t_0 is the input pulse duration equal to one PV, and t_{end} is the end time of the experiment equal to five PVs. A free outflow boundary was set as the bottom boundary as

$$D \frac{\partial C}{\partial x} = 0 \quad (5)$$

The parameters k_{att} and k_{det} were determined using inversely optimization to nZVI experimental data, whereas D was obtained from the conservative tracer results.

2.7 | Interaction energies

Interaction energies between a plate and a spherical particle with nanoscale roughness and binary charge heterogeneity have been reported in previous works (Bendersky & Davis, 2011; Bradford & Torkzaban, 2015). The interaction energies included the retarded London–van der Waals attraction, electrostatic, and Born repulsion and equations are shown in the supporting information. Four different types of colloid particle conditions were considered in interaction energy calculations in this work: (a) uniform zeta potential and smooth surface, denoted as Uniform; (b) binary charge (zeta potential) heterogeneity on a smooth surface, denoted as CH; (c) nanoscale roughness on a surface with a single zeta potential, denoted as NR; and (d) binary charge heterogeneity on a surface with nanoscale roughness, denoted as NR+CH. An illustration of these particle conditions is shown in Supplemental Figure S2. A summary of the parameters

TABLE 1 Parameters used in Derjaguin–Landau–Verwey–Overbeek (DLVO) calculation for different particle types

Type	PnZVI				PS-PnZVI			
	Uniform	CH	NR	CH+NR	Uniform	CH	NR	CH+NR
Ionic strength, mV	0.1	0.1	0.1	0.1	0.1	0.1	0.1	0.1
Particle size, nm	4,255	4,255	4,255	4,255	3,814	3,814	3,814	3,814
Zeta potential of SWI, mV	−24.52	−24.52	−24.52	−24.52	−24.52	−24.52	−24.52	−24.52
Zeta potential of the whole colloid, mV	−10.54	−52.63	−10.54	−52.63	−28.14	−52.63	−28.14	−52.63
Hamaker constant of SWI, J	8.86×10^{-20}	8.86×10^{-20}	8.86×10^{-20}	8.86×10^{-20}	8.86×10^{-20}	8.86×10^{-20}	8.86×10^{-20}	8.86×10^{-20}
Hamaker constant of nZVI, J	1×10^{-19}	1×10^{-19}	1×10^{-19}	1×10^{-19}	1×10^{-19}	1×10^{-19}	1×10^{-19}	1×10^{-19}
Hamaker constant of PANI, J	7.76×10^{-20}	7.76×10^{-20}	7.76×10^{-20}	7.76×10^{-20}	7.76×10^{-20}	7.76×10^{-20}	7.76×10^{-20}	7.76×10^{-20}
Hamaker constant of water, J	3.70×10^{-20}	3.70×10^{-20}	3.70×10^{-20}	3.70×10^{-20}	3.70×10^{-20}	3.70×10^{-20}	3.70×10^{-20}	3.70×10^{-20}
Fraction of chemical heterogeneity	0	0.7	0	0.7	0	0.7	0	0.7
Zeta potential of nZVI particles, mV	0	7.5	0	7.5	0	−17.6	0	−17.6
Fraction of nanoscale roughness	0	0	0.025, 0.05, 0.1, 0.2, 0.5	0.025, 0.05, 0.1, 0.2, 0.5	0	0	0.025, 0.05, 0.1, 0.2, 0.5	0.025, 0.05, 0.1, 0.2, 0.5
Height of nanoscale roughness, nm	0	0	100	100	0	0	100	100

Note. PnZVI, polyaniline-supported nano zero-valent iron; PS-PnZVI, phosphate-sorbed PnZVI; Uniform, uniform zeta potential and smooth surface; CH, binary charge (zeta potential) heterogeneity on a smooth surface; NR, nanoscale roughness on a surface with a single zeta potential; CH+NR, binary charge heterogeneity on a surface with nanoscale roughness; SWI, soil–water interface; PANI, polyaniline.

that were used in these interaction energy calculations is given in Table 1. Magnetic attraction can influence the aggregation behavior of PnZVI particles. The interaction energies between two particles of PnZVI were therefore also calculated by adding energy from the magnetic attraction, which is shown in the supporting information.

3 | RESULTS AND DISCUSSION

3.1 | Characterization of PnZVI and PS-PnZVI

The morphology of PnZVI that was synthesized in this study is presented in SEM and TEM images shown in Figures 1a and 1b, respectively. These images show that PnZVI has a chain-like structure and that the size of individual nZVI particles in the chain was ~ 100 nm. The EDS images of PS-PnZVI particles in Figure 1 show that phosphate was mainly adsorbed on the nZVI particles, since the element distribution of phosphorus and iron was coincident.

Kinetic and equilibrium batch experiments were conducted to assess the ability of Pn-ZVI to adsorb phosphorus. The experimental data and model results for the batch tests are

shown in Figure 2. The results of the kinetics adsorption test show that the equilibrium time was ~ 20 min and that the pseudo-second-order kinetic model can fit the data well. Results from the adsorption isotherm imply that the Langmuir model can fit the data well and that the maximum phosphorous adsorption capacity was ~ 212.8 mg g $^{-1}$. The amount of phosphorous loaded on PS-PnZVI was ~ 78.1 mg g $^{-1}$ during the synthesis process.

The zeta potential of PnZVI and PS-PnZVI was -10.54 and -28.14 mV, respectively. The adsorption of phosphate on the surface of PnZVI caused the zeta potential to become more negative because negatively charged phosphate anions were mainly adsorbed onto the surface of nZVI particles (EDS measurements in Figure 1). The initial particle size distribution of PnZVI and PS-nZVI in DI water is shown in Supplemental Figure S3. The mean particle size of PnZVI and PS-PnZVI was 4.255 and 3.814 μm , respectively, but both suspensions had a wide size distribution with particles larger than 10 μm due to aggregation. Similarly, Yu et al. (2019) reported that the particle size of surface-modified nZVI under high arsenic loading was smaller than that under low arsenic loading. This observation supports that oxyanion adsorption can cause a decrease in the size of surface-modified nZVI particles.

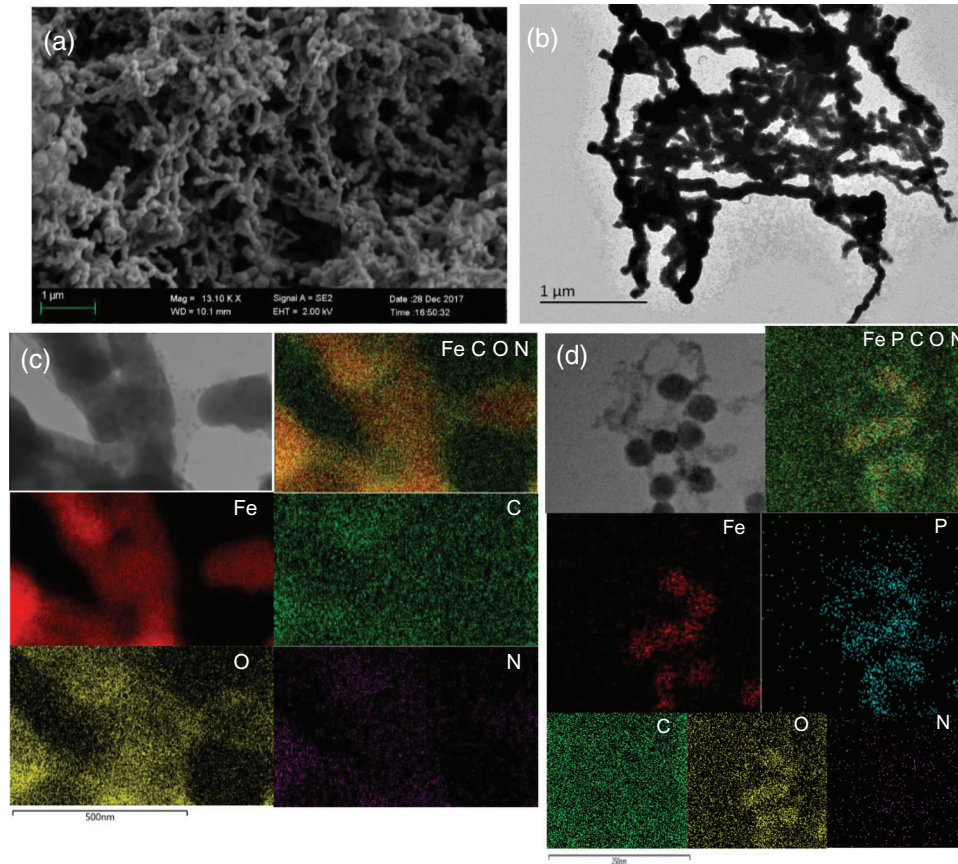


FIGURE 1 Results of scanning electron microscopy (SEM), transmission electron microscopy (TEM), and energy dispersive spectrometry (EDS) of polyaniline-supported nano zero-valent iron (PnZVI) and phosphate-sorbed PnZVI (PS-PnZVI). (a) SEM of PnZVI (b) TEM of PnZVI, (c) EDS of PnZVI, and (d) EDS of PS-PnZVI

Sedimentation studies were conducted to better assess the potential for PnZVI and PS-PnZVI suspensions to aggregate. The sedimentation curves for PnZVI and PS-PnZVI suspensions are shown in Figure 3. In this case, the relative optical absorbance of a suspension (D/D_0) is plotted as a function of time. The sedimentation curve of PnZVI declines more quickly than that of PS-PnZVI, which implies that the stability of the PnZVI was improved after the adsorption of phosphate. After 8 h, the optical density of PnZVI decreased by $\sim 91\%$, and that of PS-PnZVI decreased by $\sim 37\%$. The sedimentation curve for PS-PnZVI showed a one-region pattern, whereas that for PnZVI showed an obvious three-region pattern. Phenrat et al. (2008) reported a three-region sedimentation curve denoted as Aggregation I, Sedimentation I, and Sedimentation II and also included in situ micrographs at different times. Particles are still suspended in the Aggregation I region, even though they form chain-like aggregates. In the Sedimentation I region, the chain-like aggregates reach a critical size and sediment rapidly occurs. In the Sedimentation II region, sedimentation occurs more slowly for aggregates that did not reach the critical size. The three-region sedimentation theory therefore indicates that sedimentation of PS-PnZVI remained in the Aggregation I region, whereas the

sedimentation of PnZVI reached the Sedimentation II region after 0.4 h. The difference between the sedimentation behavior of PnZVI and PS-PnZVI can be at least partially explained by the increase of negative zeta potential after the phosphate adsorption, which increases the repulsion between particles and enhances the stability of the suspension.

Interaction energies between two PnZVI particles were calculated to better understand the cause for the observed sedimentation. These interaction energies considered van der Waals attraction, double layer repulsion, and magnetic attraction. Results shown in Supplemental Figure S4 indicate that magnetic attraction dominated that interaction energy profile and should produce massive aggregation for PnZVI. Similarly, PnZVI has been reported to have pronounced ferromagnetic properties with a saturation magnetization of $22.6 \text{ A mg}^{-2} \text{ kg}^{-1}$ (emu g^{-1}) (Bhaumik et al., 2015).

3.2 | BTCs and RPs for PnZVI and PS-PnZVI

Figure 4a shows the BTCs for PnZVI, PS-PnZVI, and a conservative tracer. The effluent concentration of PS-PnZVI

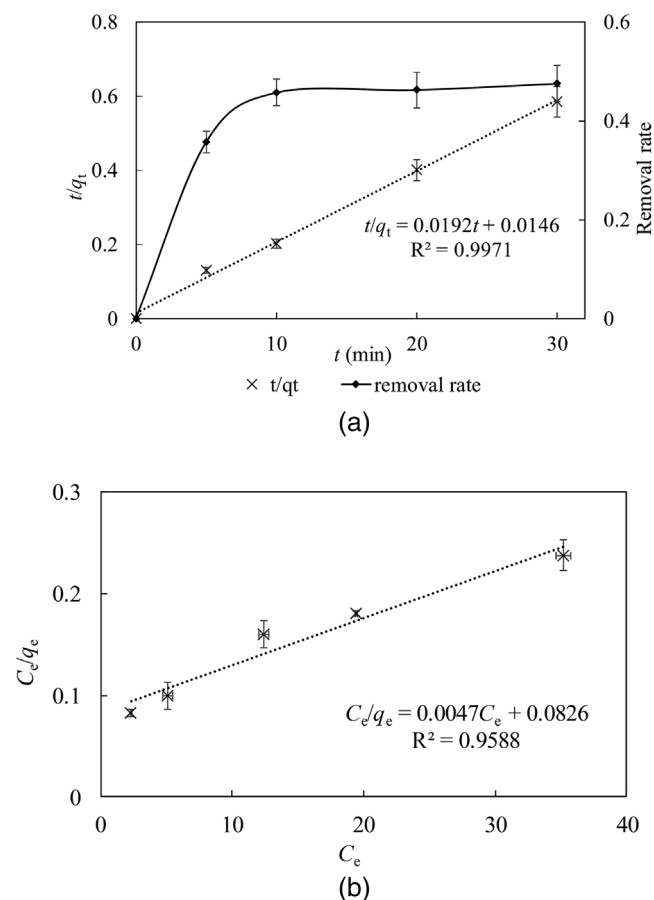


FIGURE 2 Results of batch tests of phosphate adsorption by polyaniline-supported nano zero-valent iron (PnZVI) (a) kinetics adsorption tests and (b) adsorption isotherm tests. q_t (mg g^{-1}) is the amount of phosphate sorbed by PnZVI as a function of time, C_e (mg L^{-1}) is the equilibrium concentration of phosphorous in the solution, q_{max} (mg g^{-1}) is the maximum phosphorous sorption capacity, and b (L mg^{-1}) is the Langmuir constant related to the affinity of binding sites for phosphorous

was significantly higher than that of PnZVI. About 2.5 and 53.4% of the injected mass was recovered in the column effluent for PnZVI and PS-PnZVI, respectively. The corresponding RPs for PnZVI and PS-PnZVI were determined after the recovery of the BTCs, which is shown in Figure 4b. Most of the retention for PnZVI and PS-PnZVI happened near the column inlet and RPs were hyper-exponential in shape. The main difference between PnZVI and PS-PnZVI RPs happened near the column inlet, with greater amounts of retention occurring for PnZVI than PS-PnZVI. Hyper-exponential RPs can occur as a result of straining processes such as hydrodynamic bridging and size exclusion because PnZVI and PS-PnZVI have a relatively large particle size (3–4 μm) and show potential for aggregation during transport. Sedimentation tests demonstrate that PnZVI had a higher tendency to aggregate than PS-PnZVI, and this result is consistent with a greater potential for straining. Similarly, Raychoudhury and Surasani (2017) reported that a large

particle size distribution and aggregation can contribute to straining, a decrease in porosity, and further deposition in both column tests and real field conditions. Aggregation of particles during transport has been reported to increase the deposition rate (Raychoudhury, Tufenkji, & Ghoshal, 2012).

The relative solid concentration at the bottom of the column was small for both PnZVI and PS-PnZVI. There was only a slightly higher solid concentration for PS-PnZVI than that of PnZVI in this region. This occurs because the mass of PnZVI that can pass through the column is very limited (2.5%) in comparison with PS-PnZVI (53.4%). This difference in transport can lead to more deposition near the column bottom for PS-PnZVI than PnZVI, even though the deposition rate is smaller. The PS-PnZVI can therefore transport to greater distances than PnZVI (see Figure 4).

The simulated BTCs and RPs are also shown in Figure 4 to accurately capture experimental observations ($R^2 > .95$ for PS-PnZVI and $R^2 > .94$ for PnZVI). Table 2 provides a summary of fitted retention parameters and their standard error. The dispersion coefficient (D) was determined to be $4.45 \times 10^{-7} \text{ m}^2 \text{ s}^{-1}$ by inversely fitting to the BTC of the conservative tracer ($R^2 > .98$). The values of k_{att} for PnZVI is bigger than that of PS-PnZVI, which indicates that PnZVI has a higher retention rate and capacity than PS-PnZVI. The relatively small standard error of k_{att} proves the validity of the fitting. The k_{det} for these particles was very small compared with k_{att} , and this implies that detachment of PnZVI and PS-PnZVI from the porous medium was relatively weak. Note that there is almost no tailing in the BTC (Figure 4a).

Figure 5 shows the interaction energy curves for PnZVI and PS-PnZVI with the porous medium when considering uniform properties, binary charge heterogeneity (CH), nanoscale roughness (NR), or both binary charge heterogeneity and nanoscale roughness (NR+CH) on the particle surface. All the interaction energies were divided by the product of the absolute temperature T (298 K) and Boltzmann constant k_B ($1.38 \times 10^{-23} \text{ J K}^{-1}$) to obtain dimensionless interaction energies. Supplemental Figure S2 provides an illustration of the various particle surfaces, and Table 3 presents a summary of the interaction energy parameters. The results shown in Figure 5 and Table 3 are calculated with a fraction of roughness equal to 0.2. The secondary minimum was always insignificant in the presence of the low ionic strength solution used in this study. We therefore initially focus on the ability of particles to overcome the energy barrier and enter into an attractive primary minimum. The energy barrier was very large ($>398 \text{ kT}$) when the particle surface was assumed to be smooth and chemically homogeneous. However, the presence of CH, NR, and CH+NR significantly reduced the energy barrier height. The energy barrier followed the following order for both PnZVI and PS-PnZVI: Uniform $>$ CH $>$ NR $>$ CH+NR. These results are consistent with findings from other studies that have examined the influence of CH, NR, and CH+NR on

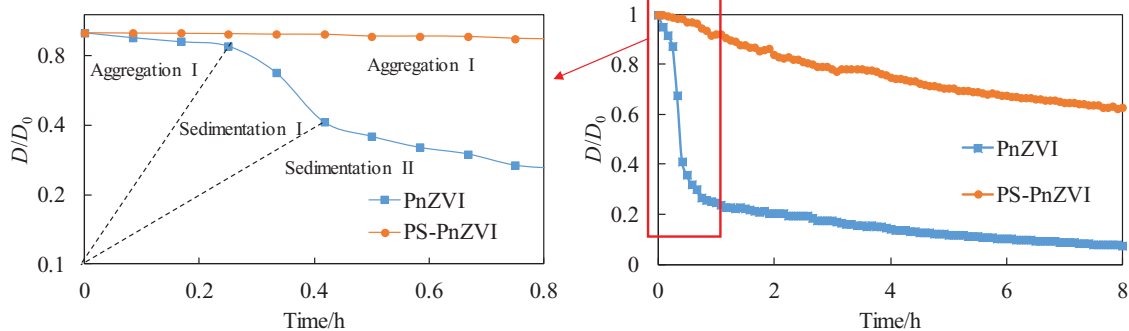


FIGURE 3 Sedimentation curves of polyaniline-supported nano zero-valent iron (PnZVI) and phosphate-sorbed PnZVI (PS-PnZVI). The D/D_0 is the relative optical absorbance of a suspension

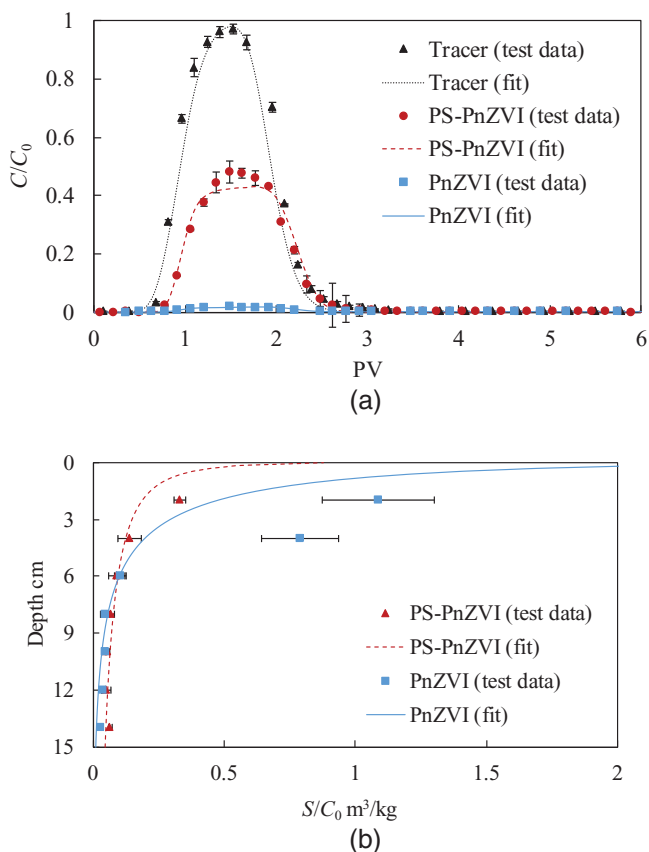


FIGURE 4 Results of the column experiments using polyaniline-supported nano zero-valent iron (PnZVI, phosphate-sorbed PnZVI (PS-PnZVI) and tracer (a) breakthrough curves (BTCs) and (b) retention profiles (RPs). PV is pore volume, C/C_0 is the relative breakthrough concentration, and S/C_0 ($\text{m}^3 \text{kg}^{-1}$) is the relative retention concentration

the energy barrier height (Bradford, Kim, Shen, Sasidharan, & Shang, 2017). Besides, a comparison of interaction energy profiles in Figures 5a and 5b reveals that PS-PnZVI always had a higher energy barrier than PnZVI due to its more negative zeta potential from adsorption of phosphate ions. This result is qualitatively consistent with the observed higher mobility for PS-PnZVI than PnZVI (Figure 4). However, the energy barrier was still always >49 kT, even when consid-

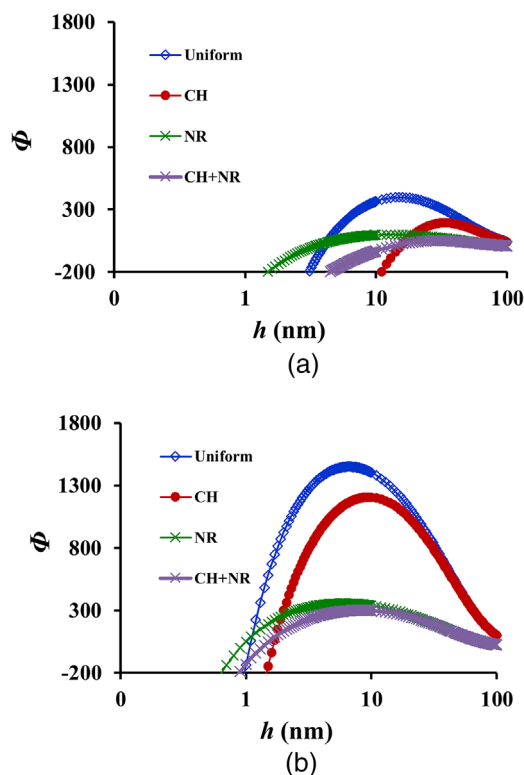


FIGURE 5 Interaction energy curves of polyaniline-supported nano zero-valent iron (PnZVI) and phosphate-sorbed PnZVI (PS-PnZVI) calculated by Derjaguin–Landau–Verwey–Overbeek (DLVO) theory: (a) PnZVI and (b) PS-PnZVI. Particle conditions include uniform zeta potential and smooth surface, denoted as Uniform; binary charge (zeta potential) heterogeneity on a smooth surface, denoted as CH; nanoscale roughness on a surface with a single zeta potential, denoted as NR; and binary charge heterogeneity on a surface with nanoscale roughness, denoted as NR+CH. Φ is the dimensionless interaction energy, and h (nm) is the distance between the particle and the solid–water interface

ering CH+NR. This energy barrier height is sufficiently high to ensure that particles will not enter the primary minimum (Shen, Bradford, Li, Li, & Huang, 2018). Consequently, these interaction energy calculations cannot provide a quantitative explanation for the observed retention behavior for PnZVI

TABLE 2 Model parameters in the advection–dispersion equation

Parameter	k_{att} –s ⁻¹ –	Standard error of k_{att}	k_{det}	Standard error of k_{det}
PnZVI	0.080	0.009	7.00×10^{-5}	1.19×10^{-4}
PS-PnZVI	0.0117	4.86×10^{-4}	3.72×10^{-5}	3.90×10^{-5}

Note. k_{att} and k_{det} are the first-order retention and release coefficients, respectively. PnZVI, polyaniline-supported nano zero-valent iron; PS-PnZVI, phosphate-sorbed PnZVI.

TABLE 3 The energy barrier and primary minimum of polyaniline-supported nano zero-valent iron (PnZVI) and phosphate-sorbed PnZVI (PS-PnZVI)

Parameter	PnZVI				PS-PnZVI			
	Uniform	CH	NR	CH+NR	Uniform	CH	NR	CH+NR
Energy barrier	–12,341.9	–17,202.4	–2,436.11	–3,409.27	–9,063.56	–11,222.3	–1,732.91	–2,165.06
Primary minimum	397.52	193.50	99.86	49.82	1,451.86	1,207.88	355.80	301.34

Note. Uniform, uniform zeta potential and smooth surface; CH, binary charge (zeta potential) heterogeneity on a smooth surface; NR, nanoscale roughness on a surface with a single zeta potential; CH+NR, binary charge heterogeneity on a surface with nanoscale roughness.

and PS-PnZVI. Results with other fraction of roughness are shown in Supplemental Table S1, which shows the decrease of energy barrier by roughness is more significant with smaller roughness fraction (Bradford et al., 2017).

Alternative explanations for PnZVI and PS-PnZVI retention include further reduction of the energy barrier height from NR and CH on the sand surface (Bradford & Torkzaban, 2013), elimination of the energy barrier in concave surface roughness locations (Shen, Li, Wang, Huang, & Jin, 2011), and physical retention mechanisms. The initial particle size distribution of PnZVI and PS-PnZVI was relatively large (Supplemental Figure S3). Furthermore, results of sedimentation tests and interaction energy calculations between PnZVI particles (Supplemental Figure S4) indicate that aggregation was occurring, especially for PnZVI in comparison with PS-PnZVI. It is likely that the large particle size and high aggregation rate of PnZVI promoted hydrodynamic bridging and straining near the column inlet (Bradford, Torkzaban, &

Walker, 2007). Results of sedimentation tests show that the tendency of PS-PnZVI to aggregate is weaker than that of PnZVI (Figure 3), and this can lead to less retention caused by bridging and straining.

3.3 | Fate of phosphate

Figure 4 demonstrated that adsorbed phosphate can enhance the mobility of PS-PnZVI in comparison with PnZVI. This implies that adsorption of an oxyanion like phosphate can be used to enhance the delivery of PnZVI to a source zone to facilitate remediation. Conversely, adsorption of oxyanion contaminants on PnZVI may also enhance their mobility. For example, phosphate was detected in the column effluent for the PS-PnZVI experiment. The phosphate BTCs are shown in Figure 6. The BTCs of phosphate (Figure 6) and PS-PnZVI (Figure 4b) almost overlap. This indicates that most of the phosphate was associated with the PS-PnZVI particles because free species of phosphate should have higher mobility than PS-PnZVI, and that desorption of phosphate from PS-PnZVI was almost negligible. This result implies a potential for PnZVI and other iron particles to facilitate the transport of oxyanion contaminants. The risks associated with these interactions are expected to be much greater for arsenate and chromate ions in comparison with phosphate (Dong et al., 2012; Dong et al., 2016), and additional research is warranted on these topics.

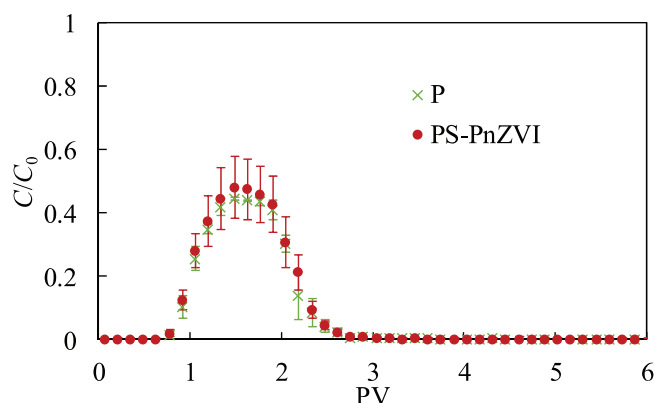


FIGURE 6 Breakthrough curves (BTCs) of phosphate and phosphate-sorbed polyaniline-supported nano zero-valent iron (PS-PnZVI). PV is pore volume, and C/C_0 is the relative breakthrough concentration

4 | CONCLUSIONS

This paper discusses the thorough characterization of surface properties, sedimentation, transport, and retention behavior of PnZVI and PS-PnZVI particles. Sedimentation and column experiments were conducted to compare the stability and

mobility of polyaniline (PANI)-supported nZVI before and after the adsorption of phosphate. Breakthrough curves and RPs were fitted by ADE to determine transport and retention parameters. Interaction energies were calculated to predict the interaction between nZVI particles and the porous medium.

The maximum adsorption capacity of PANI-supported nZVI for phosphate in DI water was 212.8 mg g⁻¹. The adsorption of phosphate on PnZVI caused a decrease in the particle size and the zeta potential became more negative, which produced an enhancement of PnZVI stability. The sedimentation process of PnZVI shows a three-region pattern, and the optical density of the suspension decreases rapidly due to the high aggregate tendency. After the adsorption of phosphate, the sedimentation process slows down due to the increase of electrical repulsion between particles.

The liquid-phase recovery rate of PS-PnZVI and PnZVI is 53.4 and 2.5%, respectively. PS-PnZVI therefore has higher mobility than PnZVI. Both of these two nZVIs show a hyper-exponential RP, and PnZVI has a higher solid concentration near the inlet than PS-PnZVI. The main retention mechanism of PnZVI and PS-PnZVI can be straining and hydrodynamic bridging due to their large aggregate size. Phosphate adsorption can enhance the mobility of PnZVI by inhibiting the aggregation tendency. These observations imply that adsorbed oxyanion contaminants (e.g., phosphate) on nZVI can potentially increase the delivery of nZVI to a contaminated source zone and may also facilitate the transport of adsorbed contaminants. The potential risks from adsorbed contaminants on nZVI should therefore be assessed in field-scale remediation applications. Additional studies are needed to evaluate the risks from the adsorption of other contaminants on nZVI under different environmental conditions.

Interaction energy calculations were conducted to better infer mechanisms of nZVI aggregation and retention in the absence and presence of adsorbed phosphate. Results showed that phosphate adsorption enhanced the energy barrier between nZVI particles and the porous medium surface. Nanoscale charge heterogeneity and roughness greatly reduced this energy barrier, but still could not explain the observed behavior. Conversely, strong aggregation of PnZVI particles was predicted due to magnetic attraction. This implies that hydrodynamic bridging and straining were the main mechanisms of PnZVI retention, and that phosphate adsorption diminished these processes by reducing particle size and aggregation. The collected information and data analyses provide new insight that allows the underlying mechanisms controlling aggregation, retention, and transport of PnZVI and PS-PnZVI to be better quantified.

ACKNOWLEDGMENTS

The National Natural Science Foundation of China (51661165015, 51979144), the Open Research Fund

Program of State key Laboratory of Hydrosience and Engineering (SKLHSE-2019-D-03), and the Research Grants Council of Hong Kong Joint Research Scheme (N_HKUST603/16) funded this research. The support provided by the China Scholarship Council (CSC) during a visit of Dantong Lin to the USDA-ARS Salinity Laboratory is acknowledged.

CONFLICT OF INTEREST

The authors declare no conflict of interest.

ORCID

Liming Hu  <https://orcid.org/0000-0001-8522-9864>

REFERENCES

- Almeelbi, T., & Bezbaruah, A. (2012). Aqueous phosphate removal using nanoscale zero-valent iron. *Journal of Nanoparticle Research*, 14(7). <https://doi.org/10.1007/s11051-012-0900-y>
- Almeelbi, T., & Bezbaruah, A. (2014). Nanoparticle-sorbed phosphate: Iron and phosphate bioavailability studies with *Spinacia oleracea* and *Selenastrum capricornutum*. *ACS Sustainable Chemistry & Engineering*, 2, 1625–1632. <https://doi.org/10.1021/sc500109v>
- Antelo, J., Avena, M., Fiol, S., López, R., & Arce, F. (2005). Effects of pH and ionic strength on the adsorption of phosphate and arsenate at the goethite–water interface. *Journal of Colloid and Interface Science*, 285, 476–486. <https://doi.org/10.1016/j.jcis.2004.12.032>
- Bendersky, M., & Davis, J. M. (2011). DLVO interaction of colloidal particles with topographically and chemically heterogeneous surfaces. *Journal of Colloid and Interface Science*, 353, 87–97. <https://doi.org/10.1016/j.jcis.2010.09.058>
- Bhaumik, M., Noubactep, C., Gupta, V. K., McCrindle, R. I., & Maity, A. (2015). Polyaniline/Fe₀ composite nanofibers: An excellent adsorbent for the removal of arsenic from aqueous solutions. *Chemical Engineering Journal*, 271, 135–146. <https://doi.org/10.1016/j.cej.2015.02.079>
- Bradford, S. A., Kim, H., Shen, C., Sasidharan, S., & Shang, J. (2017). Contributions of nanoscale roughness to anomalous colloid retention and stability behavior. *Langmuir*, 33, 10094–10105. <https://doi.org/10.1021/acs.langmuir.7b02445>
- Bradford, S. A., Šimůnek, J., Bettahar, M., van Genuchten, M. Th., & Yates, S. R. (2003). Modeling colloid attachment, straining, and exclusion in saturated porous media. *Environmental Science & Technology*, 37, 2242–2250. <https://doi.org/10.1021/es025899u>
- Bradford, S. A., & Torkzaban, S. (2013). Colloid interaction energies for physically and chemically heterogeneous porous media. *Langmuir*, 29, 3668–3676. <https://doi.org/10.1021/la400229f>
- Bradford, S. A., & Torkzaban, S. (2015). Determining parameters and mechanisms of colloid retention and release in porous media. *Langmuir*, 31, 12096–12105. <https://doi.org/10.1021/acs.langmuir.5b03080>
- Bradford, S. A., Torkzaban, S., & Walker, S. L. (2007). Coupling of physical and chemical mechanisms of colloid straining in saturated porous media. *Water Research*, 41, 3012–3024. <https://doi.org/10.1016/j.watres.2007.03.030>
- Chekli, L., Bayatsarmadi, B., Sekine, R., Sarkar, B., Shen, A. M., Scheckel, K. G., ... Donner, E. (2016). Analytical characterisation

- of nanoscale zero-valent iron: A methodological review. *Analytical Chimica Acta*, 903, 13–35. <https://doi.org/10.1016/j.aca.2015.10.040>
- Chrysikopoulos, C. V., & Syngouna, V. I. (2014). Effect of gravity on colloid transport through water-saturated columns packed with glass beads: Modeling and experiments. *Environmental Science & Technology*, 48, 6805–6813. <https://doi.org/10.1021/es501295n>
- Cirtiu, C. M., Raychoudhury, T., Ghoshal, S., & Moores, A. (2011). Systematic comparison of the size, surface characteristics and colloidal stability of zero valent iron nanoparticles pre- and post-grafted with common polymers. *Colloids and Surfaces A: Physicochemical and Engineering Aspects*, 390, 95–104. <https://doi.org/10.1016/j.colsurfa.2011.09.011>
- Crampon, M., Hellal, J., Mouvet, C., Wille, G., Michel, C., Wiener, A., ... Ollivier, P. (2018). Do natural biofilm impact nZVI mobility and interactions with porous media? A column study. *Science of the Total Environment*, 610–611, 709–719. <https://doi.org/10.1016/j.scitotenv.2017.08.106>
- Crane, R. A., & Scott, T. B. (2012). Nanoscale zero-valent iron: Future prospects for an emerging water treatment technology. *Journal of Hazardous Materials*, 211–212, 112–125. <https://doi.org/10.1016/j.jhazmat.2011.11.073>
- Dong, H., Guan, X., & Lo, I. M. (2012). Fate of As(V)-treated nano zero-valent iron: Determination of arsenic desorption potential under varying environmental conditions by phosphate extraction. *Water Research*, 46, 4071–4080. <https://doi.org/10.1016/j.watres.2012.05.015>
- Dong, H., He, Q., Zeng, G., Tang, L., Zhang, C., Xie, Y., ... Wu, Y. (2016). Chromate removal by surface-modified nanoscale zero-valent iron: Effect of different surface coatings and water chemistry. *Journal of Colloid and Interface Science*, 471, 7–13. <https://doi.org/10.1016/j.jcis.2016.03.011>
- Dong, H., & Lo, I. M. C. (2014). Transport of surface-modified nano zero-valent iron (SM-NZVI) in saturated porous media: Effects of surface stabilizer type, subsurface geochemistry, and contaminant loading. *Water, Air, & Soil Pollution*, 225(9). <https://doi.org/10.1007/s11270-014-2107-6>
- Elliott, D. W., & Zhang, W. X. (2003). Field assessment of nanoscale bimetallic particles for groundwater treatment. *Environmental Science & Technology*, 225, U971–U971. <https://doi.org/10.1021/es0108584>
- Feng, M., Qu, R., Zhang, X., Sun, P., Sui, Y., Wang, L., & Wang, Z. (2015). Degradation of flumequine in aqueous solution by persulfate activated with common methods and polyhydroquinone-coated magnetite/multi-walled carbon nanotubes catalysts. *Water Research*, 85, 1–10. <https://doi.org/10.1016/j.watres.2015.08.011>
- Hoek, E. M., Bhattacharjee, S., & Elimelech, M. (2003). Effect of membrane surface roughness on colloid–membrane DLVO interactions. *Langmuir*, 19, 4836–4847. <https://doi.org/10.1021/la027083c>
- Jiemvarangkul, P., Zhang, W. X., & Lien, H. L. (2011). Enhanced transport of polyelectrolyte stabilized nanoscale zero-valent iron (nZVI) in porous media. *Chemical Engineering Journal*, 170, 482–491. <https://doi.org/10.1016/j.cej.2011.02.065>
- Kaifas, D., Malleret, L., Kumar, N., Fetimi, W., Claeys-Bruno, M., Sergeant, M., & Doumenq, P. (2014). Assessment of potential positive effects of nZVI surface modification and concentration levels on TCE dechlorination in the presence of competing strong oxidants, using an experimental design. *Science of the Total Environment*, 481, 335–342. <https://doi.org/10.1016/j.scitotenv.2014.02.043>
- Kanel, S. R., Goswami, R. R., Clement, T. P., Barnett, M. O., & Zhao, D. (2008). Two dimensional transport characteristics of surface stabilized zero-valent iron nanoparticles in porous media. *Environmental Science & Technology*, 42, 896–900. <https://doi.org/10.1021/es071774j>
- Karn, B., Kuiken, T., & Otto, M. (2009). Nanotechnology and in situ remediation: A review of the benefits and potential risks. *Environmental Health Perspectives*, 117, 1813–1831. <https://doi.org/10.1289/ehp.0900793>
- Khan, F. I., Husain, T., & Hejazi, R. (2004). An overview and analysis of site remediation technologies. *Journal of Environmental Management*, 71, 95–122. <https://doi.org/10.1016/j.jenvman.2004.02.003>
- Kocur, C. M., Chowdhury, A. I., Sakulchaicharoen, N., Boparai, H. K., Weber, K. P., Sharma, P., ... O'Carroll, D. M. (2014). Characterization of nZVI mobility in a field scale test. *Environmental Science & Technology*, 48, 2862–2869. <https://doi.org/10.1021/es4044209>
- Li, H., Zhao, Y. S., Han, Z. T., & Hong, M. (2015). Transport of sucrose-modified nanoscale zero-valent iron in saturated porous media: Role of media size, injection rate and input concentration. *Water Science and Technology*, 72, 1463–1471. <https://doi.org/10.2166/wst.2015.308>
- Liang, Y., Bradford, S. A., Šimůnek, J., Vereecken, H., & Klumpp, E. (2013). Sensitivity of the transport and retention of stabilized silver nanoparticles to physicochemical factors. *Water Research*, 47, 2572–2582. <https://doi.org/10.1016/j.watres.2013.02.025>
- Lin, D., Hu, L., Lo, I. M. C., & Yu, Z. (2020). Size distribution and phosphate removal capacity of nano zero-valent iron (nZVI): Influence of pH and ionic strength. *Water*, 12(10). <https://doi.org/10.3390/w12102939>
- Lin, D., Zhang, Z., & Hu, L. (2019). Adsorption models of groundwater remediation by nanoscale zero valent iron. In L. Zhan, Y. Chen, & A. Bouazza (Eds.), *Proceedings of the 8th International Congress on Environmental Geotechnics* (Vol. 1, pp. 512–520). Singapore: Springer. https://doi.org/10.1007/978-981-13-2221-1_55
- Ling, L., & Zhang, W. X. (2017). Visualizing arsenate reactions and encapsulation in a single zero-valent iron nanoparticle. *Environmental Science & Technology*, 51, 2288–2294. <https://doi.org/10.1021/acs.est.6b04315>
- Macé, C., Desrocher, S., Gheorghiu, F., Kane, A., Pupeza, M., Cernik, M., ... Zhang, W.-x. (2006). Nanotechnology and groundwater remediation: A step forward in technology understanding. *Remediation Journal*, 16, 23–33. <https://doi.org/10.1002/rem.20079>
- Nagoya, S., Nakamichi, S., & Kawase, Y. (2019). Mechanisms of phosphate removal from aqueous solution by zero-valent iron: A novel kinetic model for electrostatic adsorption, surface complexation and precipitation of phosphate under oxidic conditions. *Separation and Purification Technology*, 218, 120–129. <https://doi.org/10.1016/j.seppur.2019.02.042>
- Phenrat, T., Saleh, N., Sirk, K., Kim, H.-J., Tilton, R. D., & Lowry, G. V. (2008). Stabilization of aqueous nanoscale zerovalent iron dispersions by anionic polyelectrolytes: Adsorbed anionic polyelectrolyte layer properties and their effect on aggregation and sedimentation. *Journal of Nanoparticle Research*, 10, 795–814. <https://doi.org/10.1007/s11051-007-9315-6>
- Phenrat, T., Saleh, N., Sirk, K., Tilton, R. D., & Lowry, G. V. (2007). Aggregation and sedimentation of aqueous nanoscale zerovalent iron dispersions. *Environmental Science & Technology*, 41, 284–290. <https://doi.org/10.1021/es061349a>

- Raychoudhury, T., Naja, G., & Ghoshal, S. (2010). Assessment of transport of two polyelectrolyte-stabilized zero-valent iron nanoparticles in porous media. *Journal of Contaminant Hydrology*, *118*, 143–151. <https://doi.org/10.1016/j.jconhyd.2010.09.005>
- Raychoudhury, T., & Scheytt, T. (2013). Potential of zerovalent iron nanoparticles for remediation of environmental organic contaminants in water: A review. *Water Science and Technology*, *68*, 1425–1439. <https://doi.org/10.2166/wst.2013.358>
- Raychoudhury, T., & Surasani, V. K. (2017). Implication of surface modified NZVI particle retention in the porous media: Assessment with the help of 1-D transport model. *Journal of Earth System Science*, *126*(4). <https://doi.org/10.1007/s12040-017-0836-9>
- Raychoudhury, T., Tufenkji, N., & Ghoshal, S. (2012). Aggregation and deposition kinetics of carboxymethyl cellulose-modified zero-valent iron nanoparticles in porous media. *Water Research*, *46*, 1735–1744. <https://doi.org/10.1016/j.watres.2011.12.045>
- Saberinasr, A., Rezaei, M., Nakhaei, M., & Hosseini, S. M. (2016). Transport of CMC-stabilized nZVI in saturated sand column: The effect of particle concentration and soil grain size. *Water, Air, & Soil Pollution*, *227*(10). <https://doi.org/10.1007/s11270-016-3097-3>
- Saleh, N., Kim, H. J., Phenrat, T., Matyjaszewski, K., Tilton, R. D., & Lowry, G. V. (2008). Ionic strength and composition affect the mobility of surface-modified Fe-0 nanoparticles in water-saturated sand columns. *Environmental Science & Technology*, *42*, 3349–3355. <https://doi.org/10.1021/es071936b>
- Sasidharan, S., Torkzaban, S., Bradford, S. A., Cook, P. G., & Gupta, V. (2017). Temperature dependency of virus and nanoparticle transport and retention in saturated porous media. *Journal of Contaminant Hydrology*, *196*, 10–20. <https://doi.org/10.1016/j.jconhyd.2016.11.004>
- Shen, C., Bradford, S. A., Li, T., Li, B., & Huang, Y. (2018). Can nanoscale surface charge heterogeneity really explain colloid detachment from primary minima upon reduction of solution ionic strength? *Journal of Nanoparticle Research*, *20*(6). <https://doi.org/10.1007/s11051-018-4265-8>
- Shen, C., Li, B., Wang, C., Huang, Y., & Jin, Y. (2011). Surface roughness effect on deposition of nano- and micro-sized colloids in saturated columns at different solution ionic strengths. *Vadose Zone Journal*, *10*, 1071–1081. <https://doi.org/10.2136/vzj2011.0011>
- Stutter, M. I., & Richards, S. (2012). Relationships between soil physicochemical, microbiological properties, and nutrient release in buffer soils compared to field soils. *Journal of Environmental Quality*, *41*, 400–409. <https://doi.org/10.2134/jeq2010.0456>
- Su, C., Puls, R. W., Krug, T. A., Watling, M. T., O'Hara, S. K., Quinn, J. W., & Ruiz, N. E. (2012). A two and half-year-performance evaluation of a field test on treatment of source zone tetrachloroethene and its chlorinated daughter products using emulsified zero valent iron nanoparticles. *Water Research*, *46*, 5071–5084. <https://doi.org/10.1016/j.watres.2012.06.051>
- Su, C., Puls, R. W., Krug, T. A., Watling, M. T., O'Hara, S. K., Quinn, J. W., & Ruiz, N. E. (2013). Travel distance and transformation of injected emulsified zerovalent iron nanoparticles in the subsurface during two and half years. *Water Research*, *47*, 4095–4106. <https://doi.org/10.1016/j.watres.2012.12.042>
- Sushil Raj, K., Jean-Mark, G., & Heechul, C. (2006). Arsenic(V) removal from groundwater using nano scale zero-valent iron as a colloidal reactive barrier material. *Environmental Science & Technology*, *40*, 2045–2050. <https://doi.org/10.1021/es0520924>
- Tian, Y. A., Gao, B., Silvera-Batista, C., & Ziegler, K. J. (2010). Transport of engineered nanoparticles in saturated porous media. *Journal of Nanoparticle Research*, *12*, 2371–2380. <https://doi.org/10.1007/s11051-010-9912-7>
- Tosco, T., Petrangeli Papini, M., Cruz Viggì, C., & Sethi, R. (2014). Nanoscale zerovalent iron particles for groundwater remediation: A review. *Journal of Cleaner Production*, *77*, 10–21. <https://doi.org/10.1016/j.jclepro.2013.12.026>
- Wang, C. B., & Zhang, W. X. (1997). Synthesizing nanoscale iron particles for rapid and complete dechlorination of TCE and PCBs. *Environmental Science & Technology*, *31*, 2154–2156. <https://doi.org/10.1021/es970039c>
- Wen, Z., Zhang, Y., & Dai, C. (2014). Removal of phosphate from aqueous solution using nanoscale zerovalent iron (nZVI). *Colloids and Surfaces A: Physicochemical and Engineering Aspects*, *457*, 433–440. <https://doi.org/10.1016/j.colsurfa.2014.06.017>
- Yin, K., Lo, I. M., Dong, H., Rao, P., & Mak, M. S. (2012). Lab-scale simulation of the fate and transport of nano zero-valent iron in subsurface environments: Aggregation, sedimentation, and contaminant desorption. *Journal of Hazardous Materials*, *227–228*, 118–125. <https://doi.org/10.1016/j.jhazmat.2012.05.019>
- Yu, Z. G., Hu, L. M., & Lo, I. M. C. (2019). Transport of the arsenic (As)-loaded nano zero-valent iron in groundwater-saturated sand columns: Roles of surface modification and As loading. *Chemosphere*, *216*, 428–436. <https://doi.org/10.1016/j.chemosphere.2018.10.125>
- Zhang, M., Dong, Y., Gao, S., Cai, P., & Dong, J. (2019). Effective stabilization and distribution of emulsified nanoscale zero-valent iron by xanthan for enhanced nitrobenzene removal. *Chemosphere*, *223*, 375–382. <https://doi.org/10.1016/j.chemosphere.2019.02.099>
- Zhang, Q., Liu, H., Chen, T., Chen, D., Li, M., & Chen, C. (2017). The synthesis of NZVI and its application to the removal of phosphate from aqueous solutions. *Water, Air, & Soil Pollution*, *228*(9). <https://doi.org/10.1007/s11270-017-3496-0>
- Zhang, W., Lo, I. M. C., Hu, L., Voon, C. P., Lim, B. L., & Versaw, W. K. (2018). Environmental risks of nano zerovalent iron for arsenate remediation: Impacts on cytosolic levels of inorganic phosphate and MgATP²⁻ in *Arabidopsis thaliana*. *Environmental Science & Technology*, *52*, 4385–4392. <https://doi.org/10.1021/acs.est.7b06697>
- Zhang, W. X. (2003). Nanoscale iron particles for environmental remediation: An overview. *Journal of Nanoparticle Research*, *5*, 323–332. <https://doi.org/10.1023/A:1025520116015>

SUPPORTING INFORMATION

Additional supporting information may be found online in the Supporting Information section at the end of the article.

How to cite this article: Lin D, Bradford S, Hu L, Lo IMC. Impact of phosphate adsorption on the mobility of PANI-supported nano zero-valent iron. *Vadose Zone J.* 2021;20:e20091. <https://doi.org/10.1002/vzj2.20091>